

Probabilistic seismic hazard assessments for Northern Southeast Asia (Indochina): Smooth seismicity approach

Earthquake Spectra

2020, Vol. 36(S1) 69–90

© The Author(s) 2020

Article reuse guidelines:

sagepub.com/journals-permissions

DOI: 10.1177/8755293020942528

journals.sagepub.com/home/eqs

Teraphan Ornthammarath, M.EERI¹, Pennung Warnitchai², Chung-Han Chan³, Yu Wang⁴, Xuhua Shi⁵, Phuong Hong Nguyen⁶, Le Minh Nguyen⁶, Suwith Kosuwan⁷, and Myo Thant⁸

Abstract

We present an evaluation of the 2018 Northern Southeast Asia Seismic Hazard Model (NSAHM18) based on a combination of smoothed seismicity, subduction zone, and fault models. The smoothed seismicity is used to model observed distributed seismicity from largely unknown sources in the current study area. In addition, due to a short instrumental earthquake catalog, slip rate and characteristic earthquake magnitudes are incorporated through the fault model. To achieve this objective, the compiled earthquake catalogs and updated active fault databases in this region were reexamined with consistent use of these input parameters. To take into account epistemic uncertainty, logic tree analysis has been implemented incorporating basic quantities such as ground-motion models (GMMs) for three different tectonic regions (shallow active, subduction interface, and subduction intraslab), maximum magnitude, and earthquake magnitude frequency relationships. The seismic hazard results are presented in peak ground acceleration maps at 475- and 2475-year return periods.

¹Department of Civil and Environmental Engineering, Faculty of Engineering, Mahidol University, Salaya, Thailand

²Civil and Infrastructure Engineering Department, Asian Institute of Technology, Khlong Luang, Thailand

³Department of Earth Sciences, National Central University, Taoyuan City

⁴Department of Geosciences, National Taiwan University, Taipei

⁵Earth Observatory of Singapore, Nanyang Technological University, Singapore

⁶Institute of Geophysics, Vietnam Academy of Science and Technology, Hanoi, Vietnam

⁷Active Fault Research Division, Department of Mineral Resources, Bangkok, Thailand

⁸Myanmar Earthquake Committee, Yangon, Myanmar

Corresponding author:

Teraphan Ornthammarath, Department of Civil and Environmental Engineering, Faculty of Engineering, Mahidol University, 999 Phuttamonton 4 Rd., Salaya 73170, Phuttamonton, Thailand.

Email: teraphan.orn@mahidol.edu

Keywords

Southeast Asia, seismic hazard map, PSHA, global earthquake model, smooth seismicity

Date received: 10 June 2020; accepted: 11 June 2020

Introduction

Northern Southeast Asia (NSA; or Indochina) is an area of highly diverse seismic hazard, from high seismic hazard related to the Indo-Australian and Eurasian collision plate boundary including the Myanmar oblique subduction zone to the west, to the relatively low and sparse observed seismicity inside the Sundaland plate to the east. Nevertheless, historical damaging earthquakes have also been reported inside NSA. One of the first historical records indicating damaging earthquakes in this region was from 624 B.C. (Nuttall et al., 1985); however, these historic earthquake chronicles are relatively incomplete and limited due to a paucity of historical records and scientific research. Despite a relative lack of historical seismic records, in the last decade, several moderate earthquakes ($M_w > 6.0$) of EMS-98 intensity scale ranging from VII to VIII occurred in the Lao People's Democratic Republic (PDR), Myanmar, and Thailand, creating panic among the general public and damaging local buildings and basic infrastructure. Several countries in this region have experienced a surge in economic growth in the last few decades and considerable expansion of urban areas, which could be prone to future earthquakes. Improved seismic hazard analysis results through regional efforts could lead to better understanding of seismic source characteristics in many countries in this region, which will greatly mitigate losses from future earthquakes.

Several existing probabilistic seismic hazard analysis (PSHA) maps in this region have been published in the past few decades based on the Cornell (1968) approach with different methodologies such as the conventional one where seismic sources are modeled by area sources (e.g. Vietnam, Phoung, 1991; Global, Shedlock et al., 2000; Myanmar, Thant and Kawase, 2012), or the smoothed seismicity methodology proposed by Frankel (1995; i.e. Thailand, Ornthammarath et al., 2011). However, these hazard maps have generally been independently developed as national hazard maps. The way seismic sources were modeled and the active fault parameters used were different, resulting in some significant differences in hazard values at the national boundaries. In this study, this issue was resolved by arranging several discussion meetings among key hazard analysts from various countries in NSA to come up with a consensus about seismic source modeling, active fault parameters, and appropriate ground-motion models (GMMs). The 2018 Northern Southeast Asia Seismic Hazard Model (NSAHM18) is a collaborative effort to overcome the limitation of national borders in this region. It is the regional contribution to the "Global Earthquake Model" initiative to get the consensus of relevant key persons in that region regarding current data and the state of knowledge. To achieve this objective, relevant earthquake databases and updated active fault databases in this region were reexamined and the researchers mutually decided based on recent paleoseismological studies to utilize these input parameters. The original fault parameters used in this study referred to previous studies by Phoung (1991); Fenton et al. (2003); Ornthammarath et al. (2011); Thant and Kawase (2012); and Wang et al. (2013, 2014). Additional fault parameters in Thailand are also provided by the Department of Mineral Resources (DMR). Chan et al. (2017) presented the newly compiled regional fault database used in the current study.

The NSAHM18, which was developed based on smoothed seismicity, crustal fault, and subduction zones, has been implemented in the current study. To achieve this objective, compilation of an earthquake catalog for NSA was undertaken, and the processing of the earthquake catalog is discussed. After this data preparation phase, the NSAHM18 source model for hazard computations will be further explained. The following sections describe the source models used, and the GMMs adopted, and present the results of PSHA. The assessment results include PSHA maps for the average horizontal component (as defined by Boore, 2010), peak ground acceleration (PGA), seismic hazard curves, and uniform hazard spectrum (UHS) for major cities in NSA. Only rock ($V_{s30} = 760$ m/s) ground condition, which is the standard reference site condition between NEHRP classes B and C for the construction of UHS, is reported.

Seismotectonic settings

On a continental scale, all earthquakes in NSA occur due to the continuing collision process between two plate boundaries, the Eurasian and the Indian plates. As the Indian plate is colliding with the Eurasian plate at a rate of 45 mm/year, creating a counterclockwise rotation (Billham, 2004), the Sunda Plate, comprising major parts of NSA, is moving eastward relative to the Eurasian plate with a clockwise turning of about 0.34 degrees per million years (Simons et al., 2007). The Sunda Plate's western boundary is defined by active tectonic structures, including the Arakan Thrust and Andaman Trench (Figure 1). These north–south trenches have the capacity of generating gigantic events such as the M_W 9.2, 26 December 2004 earthquake in Northern Sumatra. In addition, the dextral strike-slip Sagaing fault is believed to accommodate parts of the shear component of plate motion related to India–Eurasia convergence at 18 mm/year (Socquet et al., 2006). The greatest instrumental earthquake magnitude in NSA was the 1946 M_W 7.7 earthquake generated along the Sagaing fault. Nearly all focal mechanisms along the Sagaing fault exhibit dextral strike-slip faulting (such as the 11 November 2012 M_W 6.8 Thabeikkyin earthquake). The other main tectonic features in NSA due to the collision of the India and Eurasian plates are predominantly NW-SE and NE-SW strike-slip faults in the northern parts of Laos, Vietnam, and Thailand. Several earthquakes with $M_W > 6.0$ in this region proved that these faults are still active. Some important and well-defined active faults capable of producing earthquakes greater than 7.0 based on fault length in the NSA include the Dien Bien Phu fault (DBPF), Three Pagodas fault zones (TPFZ), Red River fault (RRF), and so on. Based on GPS and fault-trenching studies in Vietnam and the southern part of China near the RRF, the estimated slip rate of the RRF, about east of 101°E, is between 2 and 5 mm/year (Simons et al., 2007). With these slow slip rates, if one assumes that an earthquake with magnitude 7.0 is able to occur on this fault, such a large earthquake would occur every 4500–1800 years (Allen et al., 1984).

For Northwestern Myanmar, the seismicity intensifies farther to the north in Myanmar, associated with a subducting slab down to 150-km depth. Most intermediate and deep earthquakes have a strike-slip or normal focal mechanism eastward, oriented down the dip of the seismic zone. These tremors then occur within the Wadati–Benioff zone, representing its slab pull or negative buoyancy. The largest earthquake in this zone was the 1988 M_W 7.2 earthquake at 100-km depth. However, intraslab earthquakes are not normally observed below 18°N latitude, though intermediate and deep tremors have been shown to reappear at 15°N latitude propagated along the Andaman trench, and along the deformation from Nias Island north through the Andaman Islands. Figure 2 displays NSA and its surrounding seismicity map prepared from the new composite earthquake catalog from

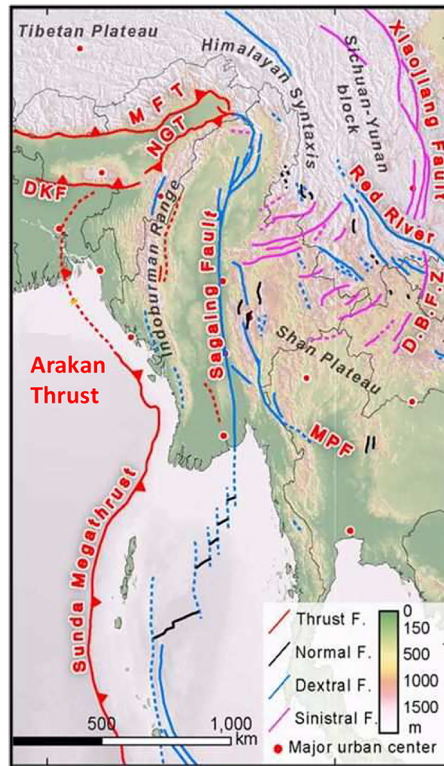


Figure 1. Major tectonic settings of NSA and major fault systems. Modified from Wang et al. (2014). DBFZ: Dien Bien Phu fault zone; MFT: Main Frontal Thrust.

1905 to 2014 for three depth intervals: shallow (less than 50 km), intermediate (between 50 and 100 km), and deep (greater than 100 km) events. The importance of the composite catalog is the fact that harmonized and updated datasets are required for PSHA.

It is clearly noticed that most parts of Myanmar are seismically active with moderate to large earthquakes. The seismicity pattern correlates well with the tectonic features as previously defined. Based on observed seismicity data in the Arakan subduction zone, the seismicity is associated with the active subduction zone where the eastward moving Indian plate is being underthrust by the Eurasian plate. The great Arakan earthquake of 1762 is the latest major rupture of the Ramree section of the Arakan megathrust. Despite a lack of major earthquakes that occurred in this area at least since 1900, the Arakan subduction zone continues to present major seismic hazards that needed to be incorporated into our analysis.

Earthquake catalog

In this study, the earthquake catalog was originally developed by Ornthammarath et al. (2011). This original catalog consists of instrumental earthquakes recorded by the Thai Meteorological Department (TMD), the USGS Determination of Epicenters on-line catalog, the International Seismological Centre (ISC), the US National Oceanic and Atmospheric Administration (NOAA), and the Global CMT catalog. The moment

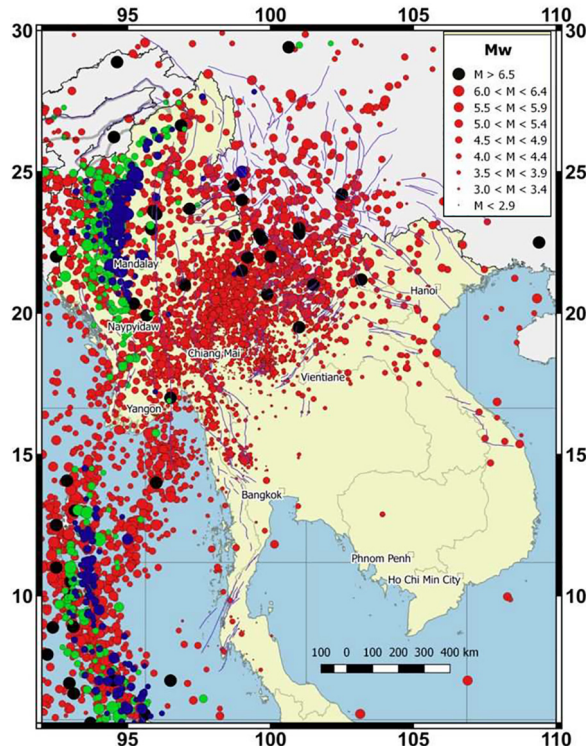


Figure 2. NSA and its declustered earthquake catalog from 1905 to 2014. Shallow events (depth ≤ 50 km) are in red circles, intermediate events ($50 < \text{depth} \leq 100$ km) are in green circles, and deep events (depth > 100 km) are in blue circles. Black circles represent shallow events with $M_W > 6.5$.

magnitude scale is adopted from 1912 to 2007. In the current work, the catalog was updated by including additional events reported by TMD from 2008 to 2014, USGS, ISC, and ISC-GEM version 4 (1904–2014; Di Giacomo et al., 2018). The TMD earthquake catalog considered here is the only local catalog since this network has just been considerably expanding following the M_W 9.2, 2004 Northern Sumatra earthquake. As of January 2018, around 80 digital seismic stations are operational and have proven to be very valuable since they are able to detect a series of small to moderate ($2 < M < 4$) tremors located mostly inside Thailand. In contrast, other seismic networks in this region have limited availability of modern digital seismic networks so it was decided that only the TMD earthquake catalog is suitable for use in this study. Therefore, the updated catalog contains earthquake records from 1905 to 2014 in a region from 0° to 30°N latitude and 88° to 110°E longitude. By increasing the observation time, recent damaging events have also been included, for example, the 2011 M_W 6.8 Tarlay earthquake, the 2012 M_W 6.8 Shwebo earthquake, and the 2014 M_W 6.1 Mae Lao earthquake.

Different earthquake magnitude scales have been identified in the combined earthquake catalog. The body-wave magnitude (m_b) and the surface wave magnitude (M_s) are normally adopted in ISC, NEIC, and other agency catalogs, while the moment magnitude (M_W) is used by the Global CMT and ISC-GEM catalogs. For the local seismic network, TMD reported only the local magnitude (M_L). To homogenize current earthquake catalogs, all different earthquake magnitude scales need to be described in terms of the

moment magnitude. For performing magnitude conversion, the magnitude scale accuracy is then ranked as follows: M_W , M_S , mb , and M_L . For events reported in terms of surface and body-wave magnitudes, the correlation of M_S and mb reported by ISC and NEIC is compared to the moment magnitude reported by the Global CMT catalog for the current study area from January 1976 to December 2014. In total, there are 28 M_S events with $5.1 \leq M_S \leq 7.0$ and $5.2 \leq M_W \leq 7.0$. For body-wave magnitude, there are 145 events with $4.3 < mb \leq 5.7$ and for $4.7 < M_W \leq 6.0$. From Figure A1, it can be seen that the M_W versus mb exponential relation proposed by Di Giacomo (2018) might overestimate M_W for events smaller than mb 5 with standard deviation of 0.16. On the other hand, the relation developed by Sipkin (2003) estimates with a lower standard deviation of 0.14. From Figure A1, it can be seen that both relations between M_S and M_W proposed by Scordilis (2006) and Di Giacomo (2018) fit quite well, with a standard deviation based on the regional dataset of 0.13. In addition, the TMD local magnitude has been compared with M_W , and the Heaton et al. (1986) relation gives a good approximation. The conversions are made using the magnitude conversion relations of Scordilis (2006) from M_S to M_W , Sipkin (2003) from mb to M_W , and Heaton et al. (1986) from M_L to M_W . Subsequently, duplicate events from different earthquake catalogs were removed to create a processed earthquake catalog. The remaining number of unduplicated events in the processed catalog turns out to be 17,534 events with magnitude equal to or greater than 3.

In addition, a declustering process is performed to remove dependent events from our catalog. First, the spatial and temporal characteristics of foreshocks and aftershocks in relation with the main shock depend very much on the magnitude of the main shock (which leads to the concept of space- and time-windows). Second, the earthquake occurrence in PSHA is assumed as a Poisson process, while in reality, the presence of aftershocks and foreshocks makes it a non-Poisson process. To adopt this approach, we will have to ignore foreshocks and aftershocks, which is justifiable since their effects are generally much less than those of the main shock. Two studies are commonly implemented: those are Gardner and Knopoff (1974) and Uhrhammer (1986). Both studies adopted the dynamic time-spatial windowing concepts with different distance and time window lengths. A comparison between declustering processes was performed. It is found that the Gardner and Knopoff (1974) method shows good conformity between observed aftershocks and known main shocks. Gardner and Knopoff's (1974) declustering method has been chosen to perform declustering analysis in the current study. Earthquake events in the catalog are divided into three depth categories: $0 < \text{depth} \leq 50$ km (shallow crustal and subduction interface), $50 < \text{depth} \leq 100$ km (subduction inslab), and $\text{depth} > 100$ km (subduction inslab). Because the declustering algorithm did not consider different hypocenter depths, the three declustering groups are computed separately considering different tectonic environments. The declustering procedure was applied to each depth subset of the catalog. This procedure eliminates about 62% of total events in the catalog. The declustered and processed catalog has 6621 earthquake events in the NSA region from 1905 to 2014 (Figure 2).

Furthermore, the completeness analysis of earthquake catalog has been adopted to determine time periods of complete data for various prescribed earthquake magnitude ranges. This standard procedure helps in computing reliable mean rates of earthquake occurrence from the earthquake catalog. Applying Gutenberg and Richter's (1954) law without considering completeness periods for different magnitude ranges will tend to underestimate the mean rates of earthquake occurrence.

Different methodologies to determine completeness periods for different magnitude ranges in the current study include the Stepp (1973) and Tinti and Mulargia (1985)

approaches. In addition, the completeness analysis is performed for smooth seismicity and area source models in this study. In total, eight seismic source models, Figures 3 and 4, are defined for this study area. These source models are determined based on their differences in seismotectonic settings, variation in observed seismicity, and quality of available instrumental data. Three of these area source models are for subduction zones SD-A, SD-B, and SD-C (Figure 4), which will be described in more detail in the subduction zones section. Two models are smooth seismicity models for shallow earthquakes (depth ≤ 50 km) in Thailand and some nearby areas (BG-1) and the remaining areas (BG-2). Note that in BG-1, the seismic monitoring network of Thailand is able to detect small earthquakes with magnitude 2–3, while in BG-2, only earthquakes with magnitude 5 or higher are well detected and recorded. The remaining two models are smooth seismicity models for intermediate earthquakes ($50 < \text{depth} \leq 100$ km; BG-Inter) and deep earthquakes (depth > 100 km; BG-Deep), which cover areas inside the Myanmar subduction slab. For each smooth seismicity and area source model, the completeness analysis is carried out independently, and due to insignificant difference between the two considered completeness analyses, the results of the Stepp (1973) approach for zones BG-1, BG-2, BG-Inter, and BG-Deep and subduction zones are presented in Table A1.

Modeling of earthquake sources

In this study, eight seismic source models are used to properly estimate seismic hazard in NSA including four smooth seismicity models, three subduction zones, and a crustal fault model. Detailed descriptions of the models are presented below.

Smooth seismicity models

Smooth seismicity models have generally been considered to evaluate seismic hazard based on locations of observed seismicity in the study region. For subareas (or regions) with no mapped active faults, such a (smooth seismicity) model accounts for all earthquakes. For other subareas with mapped faults and subduction zones, this model accounts for earthquakes smaller than the minimum earthquake magnitude of the fault and subduction source models. The smooth seismicity methodology proposed by Frankel (1995) has been utilized in this study. For this methodology, it is not required to separate the study area into subjective zones. The whole study area could be considered, but the seismicity rate is varied from locations to locations within the area depending on the earthquake locations available in the earthquake catalog. In the current study, large zones are subdivided into small grid cell, where a grid cell of 10 by 10 km² is adopted, and the number of earthquakes in each grid cell with magnitude greater than a threshold value seismicity rate is counting. Following the Ornthammarath et al. (2011) procedure, small earthquake data in BG-1 are much more completely recorded than in other zones due to high earthquake detection capability of the TMD seismic network. Therefore, the estimated seismicity rate could be improved by including small earthquakes in the hazard calculation. For the BG-1 model, the smooth seismicity rate is determined based on particularly small earthquakes (moment magnitude > 3) detected by the locally dense seismic network within Thailand. For this model, future moderate earthquakes are expected to occur in areas where a high number of low to moderate tremors have been detected. In contrast, BG-2, BG-Inter, and BG-Deep models only determine the smooth seismicity rate based on earthquakes with moment magnitude greater than 5 since moderate seismicity events in these areas are quite common; therefore, the rate could be accurately determined from events with M_W greater

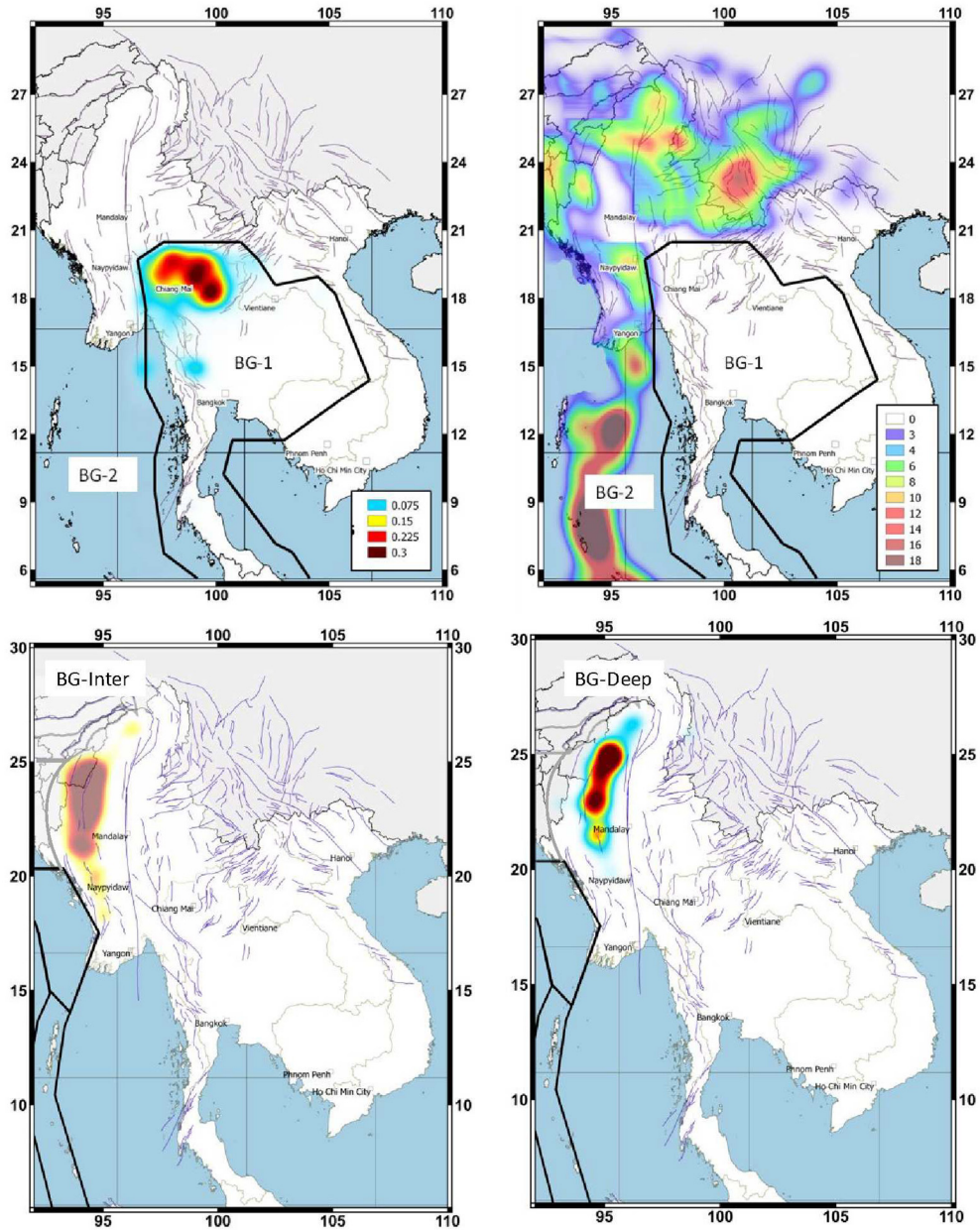


Figure 3. Shallow smoothed seismicity rates (0- to 50-km depth) inside BG-1 (top left) and BG-2 (top right), intermediate events (50- to 100-km depth; BG-Inter; bottom left), and deep events (BG-Deep; greater than 100-km depth; bottom right) in the current study. The active seismic areas are situated in the active tectonic structures such as the Sagaing fault and secondary active faults.

than 5.0. Subsequently, the seismicity rate in each grid cell is determined by the number of seismic events divided by the completeness years of each magnitude range. Later on, the

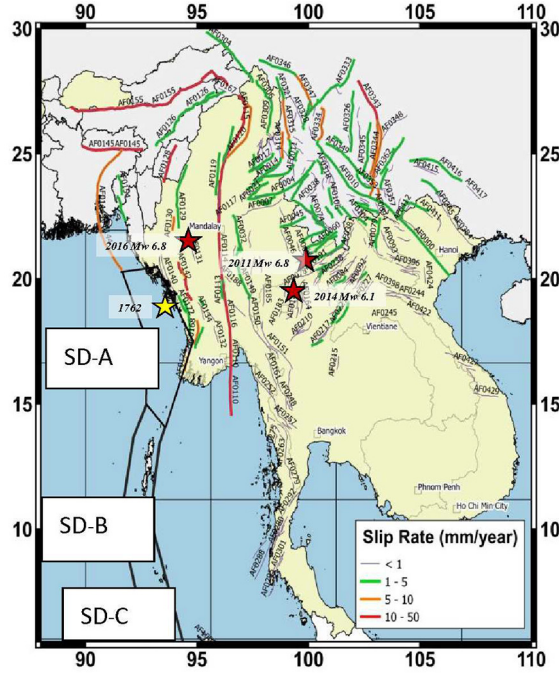


Figure 4. Faults and subduction zones considered in this study, color-coded by the slip rate (mm/year). Red stars represent recent earthquakes with recorded ground motion discussed in this study. A yellow star indicates the approximate epicenter of the 1762 Arakan earthquake from Wang et al. (2013).

computed rate is smoothed by using Gaussian smoothing by multiplying with a Gaussian function with a width given by the correlation distance C :

$$\bar{n}_i = \frac{\sum_j n_j e^{-\Delta_{ij}^2/c^2}}{\sum_j e^{-\Delta_{ij}^2/c^2}} \quad (1)$$

where \bar{n}_i is normalized to preserve the total number of events and Δ_{ij} is the distance between the i th and j th cells. The sum is taken over cells j within a distance of $3C$ of cell i . In the current study, a truncated exponential (Gutenberg–Richter (G-R)) recurrence model has been used:

$$\log_{10}(N(M_W)) = a - bM_W \quad (2)$$

where $N(M_W)$ is the mean annual rate of exceedance of earthquakes with magnitudes greater than M_W (i.e. the number of earthquake events equal to or greater than magnitude M_W per year), 10^a is the average yearly number of earthquakes of magnitude greater than or equal to zero, and b is the relative likelihood of large to small earthquakes. The b and M_{\max} values from the G-R earthquake frequency relationship are assumed to be regional constants. The correlation distance, C , is set to 50 km for computing the smoothed rate in BG-1 and 75 km for BG-2, BG-Inter, and BG-Deep. Note that, at present, there are no fixed rules or guidelines to determine an appropriate C value. If the chosen C value is too

small, the computed spatial rate will appear as a bullseye around each isolated earthquake. On the other hand, if the C value is too large, the spatial rate will be blurred and will cover areas with no seismic activity. It can be observed that the computed smoothed rate from the selected C values (Figure 3) is compatible with its corresponding pattern seismicity (Figure 2). Moreover, the selected C values are similar to those used by Frankel (1995) in making the USGS PSHA map and they are similar to the earthquake location uncertainties. The largest computed smoothed rate for BG-1 coincides with small to moderate seismicity in Northern Thailand, while, for BG-2, a high smoothed rate could be clearly observed within a high seismicity area mostly inside Myanmar. However, for southern Vietnam, a lack of small earthquakes for local and global earthquake catalogs in this area is a major problem which might be due to poor seismic network coverage and a low seismicity rate. The only seismic active source in this area is due to submarine volcanoes located off Vietnam's southeast coast.

In hazard calculations, earthquake ruptures are generated by a point source from minimum threshold magnitude up to a maximum cutoff magnitude. Each rupture is centered on the single hypocentral position. In addition, the Wells and Coppersmith (1994), WC94, and Strasser et al. (2010) relations have been used to determine lengths of finite faults for shallow and subduction intraslab models, respectively. For shallow smooth seismicity model (BG-1 and BG-2), the minimum earthquake magnitude of 4.5 will be used, while for BG-Inter and BG-Deep models, a minimum earthquake magnitude of 5.0 will be considered since earthquakes smaller than this level are less likely to cause moderate damage to structures (Bommer and Crowley, 2017). The maximum earthquake magnitude, M_{\max} , is defined as the largest earthquake that can occur in a particular seismic source. The methods to determine M_{\max} are different for each source model. A single value was assigned for shallow and subduction intraslab. Both shallow models (BG-1 and BG-2), we defined $M_{\max} = 6.5$. This value resembles the magnitude of the largest earthquakes that have occurred in low to moderate seismic region in other parts of the world (Petersen et al., 2014). In addition, earthquakes greater than 6.5 are now considered by using causative fault modeling, which will be described in fault modeling section, and it is unlikely earthquake magnitude greater than 6.5 will occur outside the mapped active faults. For BG-Inter and BG-Deep models, the M_{\max} (upper bound) equals 7.5, which is the largest reported earthquake with consideration of uncertainty by increments of 0.3. Both shallow seismicity models have the averaged depth at 7.5 km with consideration of depth distribution uncertainty assigned at 5 and 15 km with equal probability weights. For intermediate and deep seismicity models, the averaged depth is set to 75 and 125 km, respectively, and the depth distribution is assigned at 50 and 90 km and 100 and 150 km with equal probability weights, respectively.

In addition, the computed regional b -value obtained by a least squares fit to the data is 0.90, and this value is similar to the previous b -value determined in this region (Petersen et al., 2007), Figure A2. For intermediate and deep earthquakes, the computed regional b -values are 1.0 and 0.9, respectively. The estimated b -value is similar to that previously reported by Petersen et al. (2007). Because deep seismicity positions at latitude lower than 15 degrees are farther removed from much of the study area and there are different rates of observed seismicity, only the intermediate and deep seismicity inside the Myanmar subduction slab is considered in this study.

Subduction zone models

In the current study, three subduction zones are employed: the Myanmar subduction zone, SD-A, the northern Sumatra subduction zone, SD-B, and the southern Sumatra subduction zone, SD-C. These three subduction zones are delineated based on the Bird (2003) plate boundaries with reference guided by different seismic characteristic (Engdahl et al., 2007; Petersen et al., 2007). These subduction zones are modeled to rupture along an angled plane right along the Indian Eurasian tectonic subduction interface, and Table A1 shows computed G-R a - and b -values for each zone.

First, the Myanmar zone is also known as the Arakan subduction zone (Ramree section), which extends southward to Myanmar western coast. Wang et al. (2014) separate this section from the northern Chittagong area as a separate seismogenic patch because of a significant difference in the megathrust geometry. Maurin and Rangin (2010) suggest that the dip of the Chittagong section of the megathrust is nearly flat, while at the Ramree section, the dip is gently northeastward toward the coastline at an angle of about 16°. Since 1964, instrumental seismic records contain very few earthquakes greater than 6.0 on the Ramree megathrust. This might imply that it is wholly locked and the blocks above and below are accumulating strain rate of convergence of the Burma and Indian plates. Analysis of GPS data suggests that the convergence rate across the megathrust is ~ 23 mm/year at a latitude just south of the Bangladesh–Myanmar border (Socquet et al., 2006). Most of this strain is likely to be absorbed by the megathrust. However, youthful deformation of the overriding plate indicates that part of the convergence occurs across upper-plate structures within the Indo-Burman Range (Nielsen et al., 2004).

The great Arakan earthquake of 1762 is the latest major rupture of this section of the Arakan megathrust. The rupture was at least 350 km long, if one assumes that, in addition to uplift reported in the south, reported subsidence in the Chittagong region was associated with slip on the megathrust. Based on determination of the ages of marine terraces on the two major islands in this area, Wang et al. (2013) propose recurrence intervals of such 1762 tremors of around 500–700 years. For our current model, we have adopted a G-R magnitude frequency relation with parameters set by using recent paleoseismotectonic information and the earthquake catalog. Based on the G-R's parameters in Table A1, an earthquake of magnitude 8.5 would occur around every 600 years, which is consistent with recent studies of the Arakan subduction zone. For northern and southern Sumatra subduction zones (SD-B and SD-C), the computed G-R a - and b -values from observed shallow seismicity in these zones resulted in a recurrence estimate of 900 years for M 9.0 and 700 years for M 8.5 for SD-B and SD-C, respectively, similar to that from paleoseismic data as reported by Rajendran et al. (2007).

For each subduction zone, the minimum magnitude is 6.5, and the maximum magnitude equals 8.5, 9.2, and 9.2 for zone SD-A, SD-B, and SD-C, respectively. For SD-A, this maximum magnitude is equal to that of 1762 Arakan earthquake following the coastal net-uplift data with the simple megathrust model as reported in Wang et al. (2013). This is consistent with the maximum magnitude of the whole SD-A rupture zone determined from the global magnitude area relations developed for subduction interface earthquakes (Murotani et al., 2008; Papazachos et al., 2004; Strasser et al., 2010). However, the maximum magnitudes for the SD-B and SD-C subduction zones are similar to the size of the 2004 Sumatra earthquake following previous paleoseismic data reported by Zachariassen et al. (1999) and Rajendran et al. (2007). These studies concluded that the uplift of the predecessor for the great Sumatra earthquake is consistent with the magnitude of 9.2. Each subduction zone is

modeled to rupture from top (at 5 km) to bottom (at 50 km) as an inclined plane along the plate boundary (Engdahl et al., 2007). Finally, to estimate the rupture dimensions (i.e. length and width), the source scaling empirical formula for subduction interface earthquakes between moment magnitude and rupture area developed by Strasser et al. (2010) is adopted for zones SD-A, SD-B, and SD-C.

Crustal fault source model

Four hundred twenty-seven crustal fault sources are modeled in this work as shown in Figure 4. This active fault information has been reviewed and studied from recent paleoseismic investigation performed by several studies (Fenton et al., 2003; Wang et al., 2014). In addition, onshore subduction interfaces, Arakan (Dhaka domain) and Himalayan megathrusts, whose locations could be clearly defined are modeled as trace edges of the fault as defined by depth contours based on Wang et al. (2013) study. Moreover, discussions among our team members through several meetings reviewed these fault parameters before implementing them in our analysis. The fault parameters included in the current database include slip rates, locations, dips, and upper and lower depths.

In addition, the M_{\max} is estimated from each surface rupture length following the WC94 relation. For subduction zone earthquakes, the equation developed by Strasser et al. (2010) is adopted for all considered onshore subduction interfaces. In general, the strategy to assign a slip rate to each fault is based on the reliability of published studies. For example, if the results of studies are based on recent trenching investigations, those slip rates will be preferred instead of studies based on comparison of geomorphology. In addition, the rates of earthquakes in a fault model determined from the chosen slip rate and M_{\max} are directly compared with those observed from the damage or the existence of ancient structures along these faults (Ornthammarath, 2019; Wang et al., 2011). This procedure is intended to prevent estimation of the larger earthquake activity rate than the known historical record. However, it was agreed during the meetings that more research is needed to guide models of slip rates for several active faults in this region. The important properties and parameters for fault with the slip rate larger than 10 mm/year located within NSA are summarized in Table 1. All considered faults in this study are provided in the supplement file. Based on Figure 4, the Sagaing fault is clearly the largest and fastest slip rate tectonic feature in NSA. The 1400-km dextral strike-slip fault stretches from southern to northern Myanmar and joins the Himalayan syntaxes in the eastern India. Its recent slip rate, assessed from paleoseismological studies and from GPS measurements, is about 20 mm/year (Maurin and Rangin, 2010; Socquet et al., 2006).

Based on geomorphic evidence and historical seismicity, Wang et al. (2014) proposed different segments along the Sagaing fault. What distinguishes these segments are bends, splays, and distinct secondary features, as well as the terminations of historical ruptures. However, it is agreed that more research is needed to guide models of multiple segment rupture along the Sagaing fault. In the current study, the Sagaing fault model is based on Wang et al. (2014), and the slip rates for each segment vary between 12 and 20 mm/year. The M_{\max} values vary from M 7.0 to M 8.1, based on the fault segment length by using the WC94 relation.

Two assumptions are used to model earthquake recurrence behavior of these crustal faults: the characteristic earthquake and G-R models. G-R behavior means that partial fault ruptures occur with a double truncated exponential distribution of magnitudes, while characteristic behavior means that the entire fault length regularly ruptures in earthquakes

Table 1. Crustal fault source model parameters with a slip rate larger than 5 mm/year located within Northern Southeast Asia (NSA)

Fault ID	Name	Dip (°)	Width (km)	Length (km)	Characteristic earthquake magnitude		Slip rate (mm/year)	Weights of logic tree			Recurrence interval (year)			
					Min	Mean		Max	Min	Mean	Max	Min	Mean	Max
110	Sagaing fault	90	15	385	7.9	8.1	8.3	20	0.2	0.6	0.2	197	392	783
112	Sagaing fault	90	15	86	7.1	7.3	7.5	15	0.2	0.6	0.2	95	189	376
114	Sagaing fault	90	15	238	7.6	7.8	8.0	20	0.2	0.6	0.2	142	283	565
115	Sagaing fault	90	10	114	7.3	7.5	7.7	15	0.2	0.6	0.2	172	343	685
116	Sagaing fault	90	15	120	7.3	7.5	7.7	20	0.2	0.6	0.2	89	178	355
117	Sagaing fault	90	15	381	7.9	8.1	8.3	18	0.2	0.6	0.2	217	433	865
118	Sagaing fault	90	10	73	7.0	7.2	7.4	18	0.2	0.6	0.2	106	212	422
123	Sagaing fault	90	10	196	7.5	7.7	7.9	12	0.2	0.6	0.2	310	619	1236
124	Sagaing fault	90	10	65	7.0	7.2	7.4	18	0.2	0.6	0.2	97	194	388
125	Sagaing fault	90	10	64	7.0	7.2	7.4	18	0.2	0.6	0.2	97	193	385
128	Churachandpur-Mao Fault	90	5	168	7.5	7.7	7.9	16	0.2	0.6	0.2	419	836	1668
139	ELF	45	15	29	6.6	6.8	7.0	12	0.2	0.6	0.2	54	108	216
142	ELF	45	15	43	6.8	7.0	7.2	12	0.2	0.6	0.2	75	149	298
143	ELF	45	15	44	6.8	7.0	7.2	12	0.2	0.6	0.2	76	152	304
145	Dauki fault	45	35	283	7.8	8.0	8.2	11	0.2	0.6	0.2	167	333	665
155	Himalayan frontal thrust	25	40	840	8.7	8.9	9.1	15	0.2	0.6	0.2	832	1897	3315
343	Xiao Jiang	90	15	198	7.5	7.7	7.9	15	0.2	0.6	0.2	167	333	665

ELF: East-Limb fault

of a narrow magnitude range. For the G-R approach, all fault sources are assumed to generate earthquake magnitudes from M_{\min} of 6.5 to the characteristic earthquake magnitude (M_{\max}). In our fault models, the lower bound magnitude of 6.5 is adopted for the G-R model to avoid double counting effects between gridded seismicity and nearby fault zones, where the fault-based seismicity model for large magnitudes on faults that are larger than the maximum magnitude of gridded seismicity (i.e. 6.5) has been adopted (Stirling et al., 2012). In addition, the b -value of 0.90 is assumed for each fault. The chosen b -value represents an average regional b -value for the G-R relation that is consistent with previous studies (Petersen et al., 2007). The earthquake activity rate for the G-R model could be determined from the slip rate of each fault to assign the a -value from the seismic moment rate (Anderson, 1979). For the characteristic earthquake model, the earthquake recurrence interval is derived from each fault slip rate and the characteristic earthquake magnitude to be consistent with the seismic moment rate for each fault. The recurrence interval could be computed from the following: recurrence interval = $\mu \dot{u}A/M_{oc}$, where μ is the modulus of rigidity, 3.0×10^{11} dyne/cm², A is the area of the fault, \dot{u} is the assigned slip rate, and M_{oc} is the characteristic earthquake moment, which is derived from $\log(M_{oc}) = 1.5 M_{\max} + 16.05$. To account for uncertainties in the modeling of M_{\max} and earthquake magnitude frequency relationships for these crustal faults, examples of logic tree weights for these values are defined in Figure A4. Similar logic tree diagrams were also constructed for the remaining faults. The epistemic uncertainty of maximum magnitude is considered by assigning three different magnitudes ($M_{\max} - 0.2$, M_{\max} , and $M_{\max} + 0.2$) with the logic tree weights of 0.2, 0.6, and 0.2, respectively. A higher weight (0.6) is applied for values determined from the fault rupture length by using the WC94 and Strasser et al. (2010) equations for active faults and onshore subduction interfaces, respectively. It should be pointed out that the remaining weight (in total 0.4) is assigned to account for magnitude uncertainty (Petersen et al., 2014). The current set of weights was considered to be a compromise decision during our recent meeting among key stakeholders, pending future magnitude scaling relation studies in this region.

Moreover, the logic tree weights for both earthquake recurrence models are assumed to be equal (0.5 for characteristic and G-R models). This selected logic tree weight is similar to logic weights adopted by Petersen et al. (2014), and it has been discussed during our meetings that the expected ground motion through only G-R model predicts more earthquake occurrence than that the characteristic earthquake model mainly close to the minimum magnitude of 6.5 for the same fault slip rate. Therefore, when both models are adopted, each with probabilistic weight 50%, there will be more frequent occurrence of earthquakes with magnitude of about 6.5 (6.5 or higher) compared with using the characteristic model alone. While, some faults tend to produce repeatable large earthquake magnitudes, which could be explained by the characteristic model, there is limited evidence from paleoseismological studies. Until any further studies that could help to constrain our knowledge for active faults in this region, the equally assigned logic tree weights for both earthquake occurrence models is a suitable solution for this region.

GMMs

For the current study region, limited records of ground motion are available since, as previously explained, the digital seismic networks for countries in NSA have just recently been implemented. Therefore, there are few local GMMs developed for certain parts of NSA based on data from small earthquakes, and these GMMs might not be appropriate for estimation from damaging earthquakes due to different magnitude dependent decay

for ground motion observed from small versus large earthquakes (Bommer et al., 2010; Cotton et al., 2006). Although, strong ground motion data have been recorded by local seismic networks and compared with existing GMMs from three recent earthquakes in NSA with magnitude greater than 6.0 (i.e. the 2011 M_W 6.8 Tarlay earthquake in Myanmar, Ornthammarath, 2013; 2014 M_W 6.1 Mae Lao earthquake in Thailand, Ornthammarath and Warnitchai, 2016; and 2016 M_W 6.8 Chuak earthquake in Myanmar, Zaw et al., 2019), there was still debate in our recent meetings regarding their applicability for other parts of NSA where damaging ground motion has not yet been observed (e.g. southern Vietnam). However, at present, there is an agreement that the entire NSA should be considered as the same tectonic regionalization, and only existing GMMs developed for similar seismotectonic characteristics with a rigorous database, appropriated functional forms, and careful data selection should be selected (Bommer et al., 2010), while ongoing seismic monitoring is considered to be important to solve this problem in the future. In addition, the structural period ranges of chosen GMMs should be suitable for engineering requirements.

For the current study, Campbell and Bozorgnia (2014), Boore et al. (2014), and Chiou and Youngs (2014) GMMs are applied with equal logic tree weight for active shallow region including BG-1 and BG-2, and for active fault models. Comparison of recorded PGA and spectral acceleration ($T = 1.0$ s) from recent earthquakes with next generation attenuation (NGA) and NGA-W2 equations suggests that the chosen NGA-W2 GMMs provide relatively a good fit to local data over the applicable distance range from 0 to 200 km (Ornthammarath, 2013; Ornthammarath and Warnitchai, 2016). Although there is a suggestion to include additional GMMs from other databases (e.g. Europe and the Middle East), only selected NGA-W2 GMMs are considered because the current selected GMMs provide coefficients up until a 10-s structural period, which is the requirement of structural engineers.

To estimate ground motion for subduction interface GMMs, we implement three subduction interface equations. These GMMs are AB03 (Atkinson and Boore, 2003, 2008), AEA16 (Abrahamson et al., 2016; both of which are based on global data), and ZEA06 (Zhao et al., 2006; mostly based on data from Japan). These GMMs have been proven to provide a good correlation with recorded ground motion data during the recent 2010 Chile and 2011 Tohoku events. In addition, due to different attenuation rates for subduction interface earthquakes, both ZEA06 and AEA16 models have faster attenuation rates than the AB03 model. This behavior was considered to provide a good range of epistemic uncertainties (Stewart et al., 2015), since previous long distance (300 km) and large subduction interface earthquakes ($M > 7$) were widely felt by people in high-rise buildings in this region (Ornthammarath et al., 2011). Logic tree weights given to these GMMs are 0.10, 0.45, and 0.45, respectively. The AB03 global model is retained with a lower weight because the possibility of gentle decay with distance of the intermediate- to long-period motion cannot be ruled out based on previous explanations. No strong-motion data are available to guide the selection of GMMs for such earthquakes, but these models and their weights are comparable to the ones incorporated for such earthquakes in similar tectonic regions (Petersen et al., 2014). For intermediate and deep seismicity (50–100 km and >100 km, respectively), we use Atkinson and Boore (2003), Abrahamson et al. (2016), and Zhao et al. (2006) empirical relations developed from intraslab earthquakes with 0.10, 0.45, and 0.45 weight, respectively. These selected GMMs were considered appropriate since they were developed based on large databases within the same seismotectonic regions (Bommer et al., 2010). Slightly higher weights were given to AEA16 and ZEA06 due to

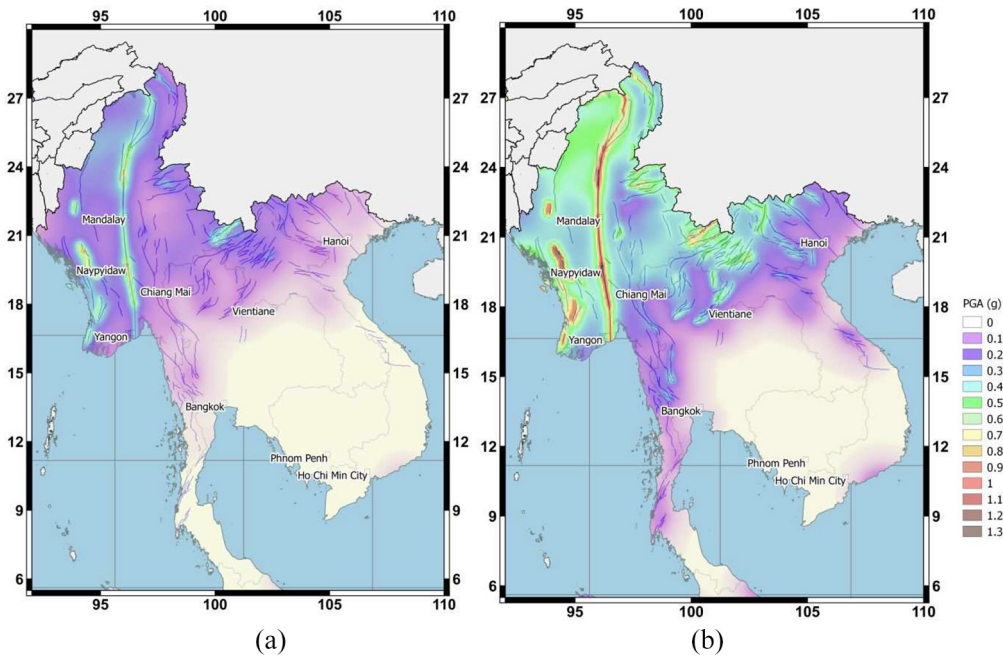


Figure 5. PSHA maps for mean PGA at (a) 475-year and (b) 2475-year return period.

the comparability of these GMMs with the measured strong motion from 2016 Chuak earthquake (Zaw et al., 2019).

Probabilistic seismic hazard results

Finally, the NSAHM18 hazard map is computed by the OpenQuake engine. We present our results as mean PGA hazard maps for 475- and 2475-year return periods, equivalent to 10% and 2% exceedance in 50 years, in Figure 5a and b, respectively. The other research outcomes of the current study are the levels of epistemic uncertainty on the seismic hazard map. The uncertainties of both quantiles (15% and 85 %) are shown in Figures A5 and A6. The computed hazard map is performed on a reference rock site condition with an average shear wave velocity in the top 30-m layer of around 760 m/s.

In general, the western part of NSA has a high seismic hazard relative to the east particularly along the Sagaing fault where faults and smoothed seismicity both dominate the seismic hazard. The NSAHM18 hazard map for PGA at the 475-year return period indicates high hazard along the fast slip rate Sagaing fault ($PGA > 0.4$ g). The contribution of the low slip rate faults in eastern Myanmar, northern Thailand, northern Laos, and northwest Vietnam to the seismic hazard is not obvious on this map. A moderate hazard level (0.1 g $< PGA < 0.25$ g), at the 475-year return period, then covers most parts of this region. This is comparable to the observed seismicity pattern (Figure 2). In contrast, the low slip rate faults become obvious in the 2475-year return period PGA map. Along the vicinity of modeled active faults, high ground motions could be clearly seen. These results verify the significance of further active fault study in this region. Of the major cities in NSA, Mandalay and Naypyidaw have clearly the highest seismic hazard, mainly due to

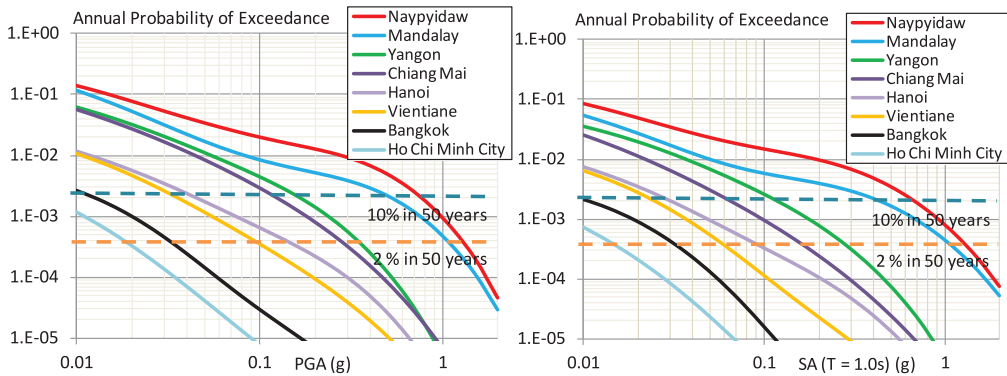


Figure 6. PGA and SA ($T = 1.0$ s) mean seismic hazard curves for eight major cities in NSA.

their adjacency to the high slip rate Sagaing fault. Their computed 2475-year return period PGAs are 0.9 and 1.2 g, respectively, and their 475-year return period PGAs are 0.5 and 0.7 g, respectively, which is comparable to the seismic hazard along the San Andreas Fault (Petersen et al., 2014). The western coast of Myanmar, the modeled subduction zone, and high slip rate active faults combine to give high hazard values with $\text{PGA} \geq 0.4$ g at the 475-year return period. The hazard in Yangon is about one-half that in Mandalay, largely because its location is about 40 km from the Sagaing fault. The deep seismicity in the northwestern part of Myanmar causes moderate hazard values ($0.25 \text{ g} < \text{PGA} < 0.30 \text{ g}$) at the 475-year return period, declining eastward toward the central part of Myanmar. This seismic hazard level is comparable to that of the Hindu Kush region in the northeastern part of Afghanistan (Boyd et al., 2007). In general, the seismic hazard contours are comparable to those in past analysis; however, some dissimilarities are observed when comparing the estimated PGA from the current work with that of previous studies. Notably, the estimated level of PGA 0.4 g near the Arakan subduction zone and the border regions of Thailand, Lao PDR, and Myanmar at the 475-year return period is about 2 times greater than the one described in the Global Seismic Hazard Assessment Program (GSHAP; Shedlock et al., 2000). The observed difference occurs because our model considers recent paleoseismic data, Maurin and Rangin (2010); Wang et al. (2013); Wang et al. (2014), that were not available or considered previously.

Figure 6 exhibits hazard curves for eight major cities of NSA: Mandalay, Naypyidaw, Yangon, Chiang Mai, Bangkok, Vientiane, Ho Chi Minh City, and Hanoi. These hazard curves show contributions from previously described seismic sources. The y-axis shows the annual probability of exceedance relative to PGA and spectral acceleration at 1.0 s on the x-axis. Based on Figure 6, major cities in this region lie in different seismic activity, and they are subjected to variable seismic hazards from high to low seismic hazard, controlling by different dominating earthquake scenarios. This information would be crucial in guiding structural engineers and disaster managers to properly prepare for future damaging earthquakes. For example, Figure A7 shows clearly that the nearby faults (e.g. the Sagaing fault) strongly dominate the total seismic hazard for both short and long periods in Naypyidaw and Mandalay. The estimated recurrence intervals of the Sagaing segment (Fault ID 112) in the southern part of Naypyidaw are relatively short, from 200 to 300 years, because slip per event for this short segment is much lower than for those

located near Mandalay. However, for Yangon, Figure A8, at short structural period, the main contributor is the Sagaing fault augmented by high background seismicity.

The hazard curve for high-rise buildings in Yangon, Figure A8, is again dominated largely by a combination of the Sagaing fault and subduction zones. Furthermore, in northern Thailand, Chiang Mai is the major urban city, and total seismic hazard seems to be comparable to that observed in Yangon; nevertheless, due to Chiang Mai's location far from active faults, background seismicity dominates significantly at short structural periods. For other major cities like Bangkok, Vientiane, and Hanoi (Figures A9 and A10) where flexible structures could be observed, the importance of active faults in defining the seismic design code could be clearly seen. In contrast, different contributions of hazard curves from active faults could be observed, indicating diverse earthquake scenarios with variable uncertainties. Deaggregation analysis is then very crucial for these major cities to fully assess different earthquake scenarios that control the hazard. Finally, Ho Chi Minh City, Figure A10, is the only location in our study where the background seismicity entirely controls seismic hazard for short and long periods due to low observed seismicity and poor tectonic information.

In addition to that mean seismic hazard curve, which has been previously discussed, UHS, the other common engineering product of PSHA, is also computed for the mean hazard and two quartiles (5th and 95th percentiles) at a 475-year return period. These full products are typically needed for engineers to constrain design ground motion values for important infrastructure. Figure A11a to d show UHS for four major cities of NSA: Mandalay, Naypyidaw, Yangon, and Chiang Mai. Although Mandalay and Naypyidaw are situated in similar tectonic settings, Naypyidaw has the greatest UHS due to its proximity to the Sagaing fault as well as the short segment previously discussed. At the 0.2 spectral period, the estimated spectral acceleration at a 475-year return period is about 1.50 g, which is 2 times larger than that predicted for Mandalay. Moreover, slightly higher uncertainty in the Naypyidaw UHS could be observed. This difference is believed to be at least partly due to seismogenic sources and GMMs. Therefore, further study should aim to assess these differences to better understand these uncertainties. In addition, a sensitivity study is needed to recognize the influence of the different uncertainties in the hazard outcomes (Douglas et al., 2014). The other interesting feature is the level of epistemic uncertainty on the UHS. By comparison of the UHSs for moderate hazard area between Yangon and Chiang Mai, it could be quickly noticed that differences in spectral shape could be observed from moderate to long structural periods ($T > 0.5$ s). This is due to the fact that seismic hazard for high-rise buildings in Yangon tends to be controlled by the Sagaing fault and the subduction zone. In addition, larger epistemic uncertainty for the Yangon UHS could be seen. This can be attributed to uncertainties in the estimates of ground motion from different tectonic environments (i.e. active shallow crust and subduction interface) and seismogenic sources, which affects the estimates of the long-period spectral acceleration.

Conclusion

Past PSHA maps in NSA had previously been assessed (i.e. Ornthammarath et al., 2011; Phoung, 1991; Thant and Kawase, 2012); however, these maps have generally been constructed on a national level with limited consideration of nearby seismogenic sources. The current study represents the first PSHA map for this region since the GSHAP by Shedlock et al., 2000. The map is based on a combination of smoothed gridded seismicity, crustal

faults, and subduction zones. The smoothed gridded seismicity model is based on available seismicity data and could be separated into four sources (BG-1, BG-2, BG-Inter, and BG-Deep). For crustal fault and subduction models, 427 crustal faults and three subduction zones have been reassessed and discussed regarding their long-term slip rates and implications toward seismic hazard results. In addition, different GMMs for three tectonic regions have been investigated and selected based on available recorded ground motion.

This study is intended to improve the current understanding of available data in this region and its effects on the computed results. PSHA maps for PGA at 10% and 2% in 50 years were drawn. Our analysis demonstrates that seismic hazard is relatively high (PGA greater than 0.4 g at 475-year return period) along the Sagaing fault and much lower (less than 0.1 g PGA at 475-year return period) for most areas inside the Sundaland plate. The area of high seismic hazard also coincides with areas of high seismicity or where major tectonic structures and active faults are located. In general, seismic hazard patterns are in comparable with previous studies; nevertheless, in the current study, the seismic hazard is mostly greater than that of Shedlock et al. (2000). This is because recent information on seismogenic source models with recurrence interval from 10^2 to 10^4 years has been incorporated in our study. Through cooperation among participants, further improvement has also been discussed, mainly on improving historical and instrumental earthquake catalogs, paleoseismological studies, and continuing ground motion monitoring for more robust GMM selection. In addition, variable seismic hazard from high to moderately low seismic hazard for major cities in NSA associated with different uncertainties could be observed. Better understanding of these factors would help to guide efforts to reduce the uncertainties in the future.

Author's note

Xuhua Shi is currently affiliated with Key laboratory of Geoscience Big Data and Deep Resource of Zhejiang Province, School of Earth Sciences, Zhejiang University, Hangzhou 310027, China.

Acknowledgments

The authors are grateful to the Editorial Board Member and two anonymous reviewers for their constructive comments that enhanced the quality of the article.

Declaration of conflicting interests

The author(s) declared no potential conflicts of interest with respect to the research, authorship, and/or publication of this article.

Funding

The author(s) disclosed receipt of the following financial support for the research, authorship, and/or publication of this article: The funding support is provided by Thailand Research Fund under contract No. RUG6030002.

Supplemental material

Supplemental material for this article is available online.

References

- Abrahamson N, Gregor N and Addo K (2016) BC hydro ground motion prediction equations for subduction earthquakes. *Earthquake Spectra* 2016; 32: 23–44.
- Allen C, Gillespie A, Yuan H, Sieh K, Buchun Z and Chengnan Z (1984) Red river and associated faults, Yunnan Province, China: Quaternary geology, slip rates, and seismic hazard. *Geological Society of America Bulletin* 95: 686–700.
- Anderson JG (1979) Estimating the seismicity from geological structures for seismic-risk studies. *Bulletin of the Seismological Society of America* 69: 135–158.
- Atkinson GM and Boore DM (2003) Empirical ground-motion relations for Subduction-zone earthquakes and their application to Cascadia and other regions. *Bulletin of the Seismological Society of America* 93: 1703–1729.
- Atkinson GM and Boore DM (2008) Erratum to empirical ground-motion relations for subduction zone earthquakes and their application to Cascadia and other regions. *Bulletin of the Seismological Society of America* 98: 2567–2569.
- Bilham R (2004) Earthquakes in India and the Himalaya: Tectonics, geodesy and history. *Annals of Geophysics* 47(2): 839–858.
- Bird P (2003) An updated digital model of plate boundaries. *Geochemistry, Geophysics, Geosystems* 4(3): 1027.
- Bommer JJ and Crowley H (2017) The purpose and definition of the minimum magnitude limit in PSHA calculations. *Seismological Research Letters* 88(4): 1097–1106.
- Bommer JJ, Douglas J, Scherbaum F, Cotton F, Bungum H and Fah D (2010) On the selection of ground-motion prediction equations for seismic hazard analysis. *Seismological Research Letters* 81(5): 783–793.
- Boore DM (2010) Orientation-independent, non geometric-mean measures of seismic intensity from two horizontal components of motion. *Bulletin of the Seismological Society of America* 100: 1830–1835.
- Boore DM, Stewart JP, Seyhan E and Atkinson GM (2014) NGA-West 2 equations for predicting PGA, PGV, and 5%-damped PSA for shallow crustal earthquakes. *Earthquake Spectra* 31: 1057–1085.
- Boyd OS, Mueller CS and Rukstales KS (2007) *Preliminary probabilistic seismic hazard map for Afghanistan*. U.S. Geological Survey Open-File Report 2007-1137. Reston, VA: U.S. Geological Survey.
- Campbell KW and Bozorgnia Y (2014) NGA-West2 ground motion model for the average horizontal components of PGA, PGV, and 5% damped linear acceleration response spectra. *Earthquake Spectra*: 30(3): 1087–1115.
- Chan CH, Wang Y, Shi X, Ornthammarath T, Warnitchai P, Nguyen PH, Nguyen LM, Kosuwan S, Thant M and Sieh K (2017) Toward uniform probabilistic seismic hazard assessments for Northern Southeast Asia. In: *AGU fall meeting San Francisco*, New Orleans, LA, 11–15 December.
- Chiou B and Youngs RR (2014) Update of the Chiou and Youngs NGA model for the average horizontal component of peak ground motion and response spectra. *Earthquake Spectra* 2014; 30: 1117–1153.
- Cornell CA (1968) Engineering seismic risk analysis. *Bulletin of the Seismological Society of America* 58: 1583–1606.
- Cotton F, Scherbaum F, Bommer JJ and Bungum H (2006) Criteria for selecting and adjusting ground-motion models for specific target applications: Applications to Central Europe and rock sites. *Journal of Seismology* 10(2): 137–156.
- Di Giacomo D, Engdahl ER and Storchak DA (2018) The ISC-GEM earthquake catalog (1904–2014): Status after the extension project. *Earth System Science Data* 10: 1877–1899. DOI: <https://doi.org/10.5194/essd-10-1877-2018>.
- Douglas J, Ulrich T, Bertil D and Rey J (2014) Comparison of the ranges of uncertainty captured in different seismic-hazard studies. *Seismological Research Letters* 85(5): 977–985.

- Engdahl RE, Villasenor A, Deshon RH and Thurber CH (2007) Teleseismic relocation and assessment of seismicity (1918–2005) in the region of the 2004 Mw 9.0 Sumatra-Andaman and 2005 MW 8.6 Nias Island Great Earthquakes. *Bulletin of the Seismological Society of America* 97(1A): S43–S61.
- Fenton CH, Charusiri P and Wood SH (2003) Recent paleoseismic investigations in northern and western Thailand. *Annals of Geophysics* 46: 957–981.
- Frankel A (1995) Mapping seismic hazard in the Central and Eastern United States. *Seismological Research Letters* 66: 8–21.
- Gardner JK and Knopoff L (1974) Is the sequence of earthquakes in southern California, with aftershocks removed, Poissonian? *Bulletin of the Seismological Society of America* 64: 1363–1367.
- Gutenberg B and Richter C (1954) *Seismicity of the Earth and Associated Phenomena*. Princeton, NJ: Princeton University Press.
- Heaton TH, Tajima F and Mori AW (1986) Estimating ground motions using recorded accelerograms. *Surveys in Geophysics* 8: 25–83.
- Maurin T and Rangin C (2010) Structure and kinematics of the Indo-Burmese Wedge: Recent and fast growth of the outer wedge. *Tectonics* 28: TC2010.
- Murotani S, Miyake H and Koketsu K (2008) Scaling of characterized slip models for plate-boundary earthquakes. *Earth Planets Space* 60: 987–991.
- Nielsen C, Chamot-Rooke N and Rangin C (2004) From partial to full strain partitioning along the Indo-Burmese hyper-oblique subduction. *Marine Geology* 209: 303–327.
- Nutalaya P, Sodsri S and Arnold EP (1985) *SEASSEE Series on Seismology, vol. II—Thailand, Southeast Asia Association of Seismology and Earthquake Engineering and USGS*. Denver, CO: United States Geological Survey.
- Ornthammarath T (2013) A note on the strong ground motion recorded during the Mw 6.8 earthquake in Myanmar on 24 March 2011. *Bulletin of Earthquake Engineering* 11: 241–254.
- Ornthammarath T (2019) Seismic damage to ancient monuments in Chiang Saen (Northern Thailand): Implication for historical earthquakes in Golden Triangle area. *Philosophical Transactions of the Royal Society A* 377: 2018025.
- Ornthammarath T and Warnitchai P (2016) The 5 May 2014 MW 6.1 Mae Lao (Northern Thailand) earthquake: Interpretations of recorded ground motion and structural damage. *Earthquake Spectra* 32: 1209–1238.
- Ornthammarath T, Warnitchai P, Worakanchana K, Zaman S, Sigbjörnsson R and Lai CG (2011) Probabilistic seismic hazard assessment for Thailand. *Bulletin of Earthquake Engineering* 9: 367–394.
- Papazachos B, Scordilis E, Panagiotopoulos D, Papazachos C and Karakaisis G (2004) Global relations between seismic fault parameters and moment magnitude of earthquakes. *Bulletin of the geological society of Greece* 36(3): 1482–1489. doi:<https://doi.org/10.12681/bgsg.16538>
- Petersen M, Harmsen S, Mueller C, Haller K, Dewey J, Luco N, Crone A, Lidke D and Rukstales K (2007) Documentation for the Southeast Asia Seismic Hazard Maps. Administrative Report, U.S. Geological Survey, Reston, VA, 65 pp.
- Petersen MD, Moschetti MP, Powers PM, Mueller CS, Haller KM, Frankel AD, Zeng Y, Rezaeian S, Harmsen SC, Boyd OS, Field N, Chen R, Rukstales KS, Luco N, Wheeler RL, Williams RA and Olsen AH (2014) *Documentation for the 2014 update of the United States national seismic hazard maps*. U.S. Geological Survey Open-File Report 2014–1091. Denver, CO: U.S. Geological Survey, 243 pp.
- Phoung NH (1991) Probabilistic assessment of earthquake hazard in Vietnam based on seismotectonic regionalization. *Tectonophysics* 198: 81–93.
- Rajendran CP, Rajendran K, Anu R, Earnest A, Machado T, Mohan PM and Freymueller J (2007) Crustal deformation and seismic history associated with the 2004 Indian Ocean earthquake—A perspective from the Andaman-Nicobar Islands. *Bulletin of the Seismological Society of America* 97: S174–S191.
- Scordilis EM (2006) Empirical global relations converting MS and mb to moment magnitude. *Journal of Seismology* 10: 225–236.

- Shedlock KM, Giardini D, Grünthal G and Zhang P (2000) The GSHAP global seismic hazard map. *Seismological Research Letters* 71: 679–689.
- Simons W, Socquet A, Vigny C, Ambrosius B, Haji Abu S, Promthong C, Subarya C, Sarsito DA, Matheussen S, Morgan P and Spakman W (2007), A decade of GPS in SE Asia: Resolving Sundaland motion and boundaries. *Journal of Geophysical Research* 112: B06420. DOI: <https://doi.org/10.1029/2005JB003868>
- Sipkin SA (2003) A correction to body-wave magnitude mb based on moment magnitude MW. *Seismological Research Letters* 74(6): 739–742.
- Socquet A, Vigny C, Chamot-Rooke N, Simons W, Rangin C and Ambrosius B (2006) India and Sunda plates motion and deformation along their boundary in Myanmar determined by GPS. *Journal of Geophysical Research* 111: B05406.
- Stepp JC (1973) *Analysis of completeness of the earthquake sample in the Puget Sound area* (ed Harding ST). Seismic Zoning, NOAA Technical Report ERL 267-ESL30, Boulder, CO: NOAA.
- Stewart JP, Douglas J, Javanbarg M, Bozorgnia Y, Abrahamson NA, Boore DM, Campbell KW, Delavaud E, Erdik M and Stafford PJ (2015) Selection of ground motion prediction equations for the global earthquake model. *Earthquake Spectra* 31(1): 19–45.
- Stirling MW, McVerry GH, Gerstenberger MC, Litchfield NJ, Van Dissen RJ, Berryman KR, Barnes P, Wallace LM, Villamor P, Langridge RM, Lamarche G, Nodder S, Reyners, ME, Bradley B, Rhoades DA, Smith WD, Nicol A, Pettinga J, Clark KJ, Jacobs K (2012) National seismic hazard model for New Zealand: 2010 update. *Bulletin of the Seismological Society of America* 102(4): 1514–1542; doi:10.1785/0120110170
- Strasser FO, Arango MC and Bommer JJ (2010) Scaling of the source dimensions of interface and intraslab subduction-zone earthquakes with moment magnitude. *Seismological Research Letters* 81: 941–950.
- Thant M and Kawase H (2012) Seismic sources identification and characterization for Myanmar: Towards updating the probabilistic seismic hazard maps. In: *AGU Fall meeting*, San Francisco, CA, 14–18 December 2015.
- Tinti S and Mulargia F (1985) Completeness analysis of a seismic catalog. *Annals of Geophysics* 3: 407–414.
- Uhrhammer R (1986) *Characteristics of northern and southern California seismicity: Earthquake notes*, v. 57, p. 21.
- Wang Y, Shyu JBH, Sieh K, Chiang H-W, Wang C-C, Aung T, Lin Y-NN, Shen C-C, Min S, Than O, Lin KK and Tun ST (2013) Permanent upper plate deformation in western Myanmar during the great 1762 earthquake: Implications for neotectonic behavior of the northern Sunda megathrust. *Journal of Geophysical Research-Solid Earth* 118: 1277–1303.
- Wang Y, Sieh K, Aung T, Min S, Khaing SN and Tun ST (2011) Earthquakes and slip rate of the southern Sagaing fault: Insights from an offset ancient fort wall, lower Burma (Myanmar). *Geophysical Journal International* 185(1): 49–64.
- Wang Y, Sieh K, Tun ST, Lai KY and Myint T (2014) Active tectonic and earthquake Myanmar region. *Journal of Geophysical Research* 119: 3767–3822.
- Wells DL and Coppersmith KJ (1994) New empirical relationships among magnitude, rupture length, rupture width, and surface displacements. *Bulletin of the Seismological Society of America* 84(4): 974–1002.
- Zachariassen J, Sieh K, Taylor FW, Edwards RL and Hantoro WS (1999) Submergence and uplift associated with the giant 1833 Sumatran subduction earthquake—Evidence from coral microatolls. *Journal of Geophysical Research* 104: 895–919.
- Zaw SH, Ornthamarath T and Poovarodom N (2019) Seismic reconnaissance and observed damage after the Mw 6.8, 24 August 2016 Chauk (Central Myanmar) earthquake. *Journal of Earthquake Engineering* 23(2): 284–304.
- Zhao JX, Zhang J, Asano A, Ohno Y, Oouchi T, Takahashi T, Ogawa H, Irikura K, Thio H, Somerville P, Fukushima Y and Fukushima Y (2006) Attenuation relations of strong ground motion in Japan using site classification based on predominant period. *Bulletin of the Seismological Society of America* 96(3): 898–913.